AD_____

(Leave blank)

Award Number: W81XWH-08-1-0152

TITLE: Portable Ultrasound Imaging of the Brain for Use in Forward Battlefield Areas

PRINCIPAL INVESTIGATOR: Gregory T. Clement

CONTRACTING ORGANIZATION: UltraDiagnostics, Inc.

Attleboro Falls, MA 02763

REPORT DATE: March 2009

TYPE OF REPORT: Annual

PREPARED FOR: U.S. Army Medical Research and Materiel Command

Fort Detrick, Maryland 21702-5012

DISTRIBUTION STATEMENT:

Approved for public release; distribution unlimited

REPORT DOCUMENTATION PAGE

Form Approved
OMB No. 0704-0188

1. REPORT DATE *(DD-MM-YYYY*	2. REPORT TYPE	3. DATES COVERED *(From - To)*
30-03-2009	Annual	31 Mar 2008 – 28 Feb 2009

4. TITLE AND SUBTITLE
Portable Ultrasound Imaging of the Brain for Use

In Forward Battlefield Areas

5a. CONTRACT NUMBER

5b. GRANT NUMBER
W81XWH-08-1-0152

5c. PROGRAM ELEMENT NUMBER

6. AUTHOR(S)
Gregory T. Clement

5d. PROJECT NUMBER

5e. TASK NUMBER

5f. WORK UNIT NUMBER

7. PERFORMING ORGANIZATION NAME(S) AND ADDRESS(ES)

UltraDiagnostics, Inc.
PO Box 1375 Attleboro Falls,
MA 02763

8. PERFORMING ORGANIZATION REPORT NUMBER

9. SPONSORING / MONITORING AGENCY NAME(S) AND ADDRESS(ES)
U.S. Army Medical Research
and Materiel Command
Fort Detrick, Maryland 21702-5012

10. SPONSOR/MONITOR'S ACRONYM(S)

11. SPONSOR/MONITOR'S REPORT NUMBER(S)

12. DISTRIBUTION / AVAILABILITY STATEMENT

Approved for public release; distribution unlimited

13. SUPPLEMENTARY NOTES

14. ABSTRACT Using ultrasound as a detection device in the body, including the brain, has been extensively investigated. Unfortunately, previous ultrasound-based methods in the brain have suffered from the severe distortion caused by the skull bone. However, we have recently developed a technique that allows ultrasound to propagate through the skull with significantly reduced distortion, using a shear mode technique. *The current project will develop a device for non-invasive identification of the presence of foreign bodies inside the skull*, and localization of such objects within the skull, will be lightweight, portable, durable, battery-operated, easy to use and appropriate for effective and practical battlefield use in forward areas. The finished device will operate in two modes: In the first mode it will function as a hand-held device, powered by AA batteries. In this mode it will provide a simple yes/no indication on the presence of foreign bodies as a function of location in the brain. In the second mode, the same device will also be capable of interfacing with laptop computer via USB interface. In this mode imaging and analysis software will form an image of regions in the brain, which can be interpreted by a medic or relayed to a remote medical professional for evaluation.

15. SUBJECT TERMS
Ultrasound, Portable Diagnostic Device, Brain Monitoring

16. SECURITY CLASSIFICATION OF: U			17. LIMITATION OF ABSTRACT	18. NUMBER OF PAGES	19a. NAME OF RESPONSIBLE PERSON
a. REPORT	b. ABSTRACT	c. THIS PAGE	UU	20	USAMRMC
					19b. TELEPHONE NUMBER *(include area code)*

TABLE OF CONTENTS

INTRODUCTION

The overall goal of the project is to develop a portable noninvasive device capable of providing information relevant to the detection of foreign bodies in the brain. The initial stage throughout the first year of funding has focused primarily on performing *in vitro* target and transducer characterization measurements, developing signal processing techniques for data analysis, and performing *in vitro* volumetric interrogation evaluation. These initiatives will provide necessary input and information for developing a portable version of the ultrasound device for foreign body detection. The following report has divided sub-parts of the project in to four initiatives for more straightforward referencing.

The first two initiatives concentrate on better understanding propagation effects through the skull, as the multi-layered bone structure in the skull introduces significant distortion and attenuation to the ultrasound signal. This work builds upon our previous work on this issue [1][2][3][4], but applies it directly to the present task of a simple rapid detection device. These effects contribute to poor signal quality when scattering off a foreign body is considered and require both thorough experimental evaluation of scattering surfaces within the skull and signal processing to resolve the scattered signal amidst the noise. The third initiative is designed to optimize the placement and number of transducers required to interrogate the maximize volume within the skull. An underlying goal of this project is to simplify the device construction and operation. These two aspects will be best served by minimizing the number of transducers, resulting in an optimization between transducer number and effective interrogation volume. The fourth initiative addresses the technical objective of this phase in the project: to design and construct a low-cost and portable multi-channel ultrasound pulser-receiver that would drive the ultrasound transducers and feed the signals to an analyzer. This system improves upon a previously-constructed ultrasound single-channel pulser-receiver systems. Multiple channels can now be used for detection from several transducers positioned around the skull for comprehensive brain imaging. In this period, a pulse generator was constructed and connected to the multiplexer to allow for selective excitation between as many as six transducers. For reference, relevant milestones are cited, as presented in the original grant proposal. These milestones are provided in the Appendix.

BODY

Initiative 1: In vitro target and transducer characterization

Milestones 1, 2, 8

Studies were performed on ex vivo human skulls (Brigham and Women's Hospital Discarded Tissues protocol 1999P00217), which are degassed and stored in Formalin. Our past research [5] has shown that the properties of these preserved skulls is acoustically similar to fresh samples. Degradatory trans-cranial propagation effects pose a transducer design tradeoff scenario with imaging resolution, as distortion and

attenuation effects become more pronounced for higher ultrasound frequencies, while imaging resolution is improved at higher frequencies. Transducer diameter is an additional transducer design parameter that impacts signal quality. These two design parameters (transducer frequency and diameter) have been evaluated in a series of backscatter scan measurements in order to optimize the transducer design. While we have four transducers currently available in our laboratory, the results from these measurements helped inform the future purchase of additional transducer ceramics for further evaluation of frequency and diameter.

Listed by center frequency and element diameter, the four transducers tested were: 1 MHz, 0.5" (V303, Panametrics-NDT Corp., Waltham MA); 0.5 MHz, 1.1" (M2008, Panametrics-NDT Corp); 0.5 MHz, 0.75" (V318, Panametrics-NDT Corp.); 0.25 MHz, 2" (in-house construction). With the exception of the fourth transducer which was weakly focused and possessed a narrow bandwidth, the transducers were chosen since they were planar and broadband, providing a maximum beamwidth along the acoustic axis and optimal axial resolution. The transducers were separately evaluated by positioning the transducer in a tank filled with deionized water. Also present in the tank was a human skull cap and a 2.78-mm diameter stainless steel sphere. The skull and transducer were fixed while the sphere was attached to a computer-controlled positioning system (Velmex, Mineola NY). The transducer was positioned perpendicular to the skull outer surface and was excited by a high-amplitude 2.5-cycle pulse generated by a pulser-receiver unit (5072, Panametrics-NDT Corp.). Reflection impingent back to the transducer was received by the pulser-receiver as well. The pulse repetition frequency (PRF) was 500 Hz, the excitation energy level was 4, and the receive gain was +30 dB. The signal from the pulser-receiver was digitized at 10 Msamples/s with an 8-bit oscilloscope (TDS 3014B, Tektronix Inc., Richardson, TX) and saved to a computer for analysis.

The sphere target was positioned inside the skull, approximately 90 mm from the transducer, and moved in 1-mm steps in a raster scan pattern along a plane parallel to the transducer surface. The signal return from the transducer was acquired at each position. With the exception of the low-bandwidth 0.25-MHz transducer, a scan was conducted for each transducer, where the transducer acoustic axis was perpendicularly aligned in four positions relative to the skull: the front; side; top (above the suture); and in the free field, where no skull was present. The 0.25-MHz transducer was found to have insufficient signal sensitivity and was not evaluated at each position.

Following the measurements, the data was analyzed to determine the -6-dB area over which the target was apparent in the signal. This was accomplished by determining the magnitude of the signal at the transducer center frequency for each waveform and subsequently compiling an image of the signal magnitude the corresponded to its spatial position in the scan. Shown in Fig. 1, the area represents the spatial region over which the target is apparent and provides an indication of the spatial sensing efficacy of each transducer and position relative to the skull. The V318 transducer contained the largest area over which the target was detected. This result was expected, given the greater attenuation at 1 MHz and the lower sensitivity of the larger-aperture M2008 transducer.

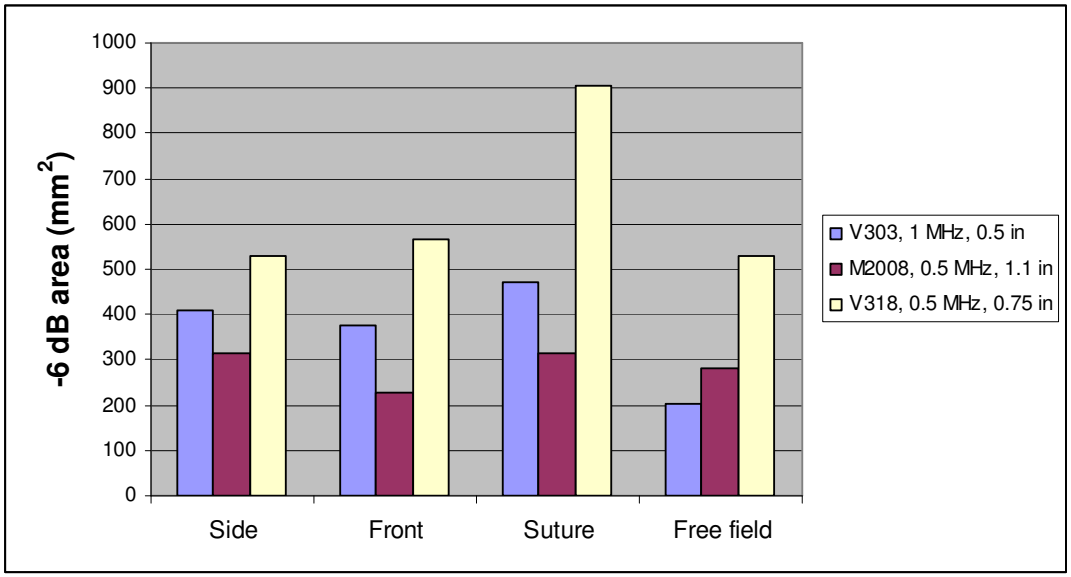

Figure 1: -6-dB backscattered area per position and transducer.

Based on this result we chose to use the V318 transducer for the remaining experimental initiatives that follow (see Initiative 3). Additionally, we will evaluate the efficacy of using other sub-megahertz frequencies and of varying transducer diameter. We recently placed and received the first shipment order of piezoelectric ceramics that feature a nominal center frequency of 0.32 and 0.8 MHz. These ceramics have been wired and backed, and will soon undergo testing with a pulser-receiver system.

Initiative 2: Signal processing

Milestone 5

The adopted approach is to develop multiple detection mechanisms based on different scan measurements, such as described in Initiative 1. Initially, these mechanisms are to be implemented and tested independently to better define default values and threshold parameters such that the mechanism can be operated robustly for several echo scans collected under different experiment arrangements (object shapes and sizes, transducer characteristics, acoustic environments, etc). Once a certain confidence level is achieved, these detection mechanisms will be combined in a voting scheme to provide a reliable decision about the existence and location of an object, if present. The echo scan to be inspected for the existence of an object needs to be pre-processed before going through any of the developed detection mechanisms, as briefly outlined below.

Preprocessing

1. An echo scan from a spherical target in the presence of the skull in a particular orientation is selected.
2. This echo is first conditioned by removing the base background signal by subtracting a reference scan that contains echo signals as reflected from the skull without a foreign object present in the signal.

Detection Mechanisms

Three different detection mechanisms were implemented and being tested, fine tuned and verified. The mechanisms are:

1. Entropy-Based Mechanism: This approach applies some signal conditioning techniques including smoothing and filtering, then uses the calculated energy "entropy-like" in a given scan to detect, if any, the existence of an object (spherical target in our case, bullet fragment for the particular project) and to locate the detected object (s).

Pros/Cons:

- It needs a robust tuning methodology to better select default thresholds and parameters in use (include several ad-hoc trials and carefully examination for the experiment set-up)
- It doesn't need a reference scan, less demanding.

2. Correlation-Based Mechanism: This mechanism applies cross-correlation techniques along with signal conditioning to predict the existence and location of the object, if any, in a given scan. This technique needs a reference scan that represents target-exist data set to be cross correlated with the given scan to be searched for an object.

Pros/Cons:

- It does need a reference scan.
- Fewer (yet need) parameters and thresholds to be tuned as default values.

3. Frequency-Based Mechanism: In this approach several techniques to compute the frequency content of a given scan are used to better locate the object, if present. The knowledge of the fundamental frequency for the operating transducer is crucial. The techniques under consideration include Fourier Series Coefficients, Fast Fourier Transform for the scan as whole and for windowed- segment of the scan. An amplitude 2D XY images along the acoustic axis (z-axis) in the frequency domain is tested for the existence of an object and an XY 1D profile is studied to locate the object, if present, by locating the maximum of the profile.

Pros/Cons:

- It does need the knowledge of the Transducer Fundamental Frequency
- Virtually no parameters and thresholds need to be tuned.

Next Step

These detection mechanisms need to be integrated into one unified framework. The overall performance of the combined detection algorithm will be more robust and reliable. The combined mechanisms need to be tested further and verified for several echo scans collected under different experiment and apparatus setups. Other detection mechanisms will be developed, implemented and tested. At any stage detection mechanism are to operate initially in competing basis then in a complementary fashion.

Recommendations

More echo scans are needed to validate developed detection mechanisms (consistent with general class of numerical observer algorithms). Echo scans for the brain for animals or humans will be of great interest and value, in particular to provide a base background echo signal.

Initiative 3: Volumetric interrogation evaluation

Milestones 2, 8

An additional key design aspect is to determine the number of transducers involved in the array and optimal positions around the skull to ensure a maximal interrogation volume. In order to maintain a lightweight design and minimal power consumption we seek to minimize the number of transducers. Also, to reduce the system complexity we must determine how best to minimize the operator interaction with the array positioning and control before and during the measurement.

Most transcranial diagnostic ultrasound procedures rely on regions of the skull that are known to have a relatively-thin thickness in order to reduce attenuation effects, regions referred to as acoustic windows. For this reason, most procedures rely on transmission through the temporal bone. Interrogation through this region will only provide a limited volume, however, so it is important to evaluate different positions on the skull to create a comprehensive volumetric map of where the sound will penetrate through the skull into the brain. Understanding that biological variability is quite large in the skull, this map will provide a rough idea of the effective coverage that may be obtained, as well as provide feedback on the number of transducers required for the end device and where they should be positioned relative to the skull.

Working with the V318 (0.5 MHz, 0.75” diameter) transducer, six different positions were evaluated on two separate skulls, the skull cap described in Initiative 1 and a skull that is cut down the midline. As before, the skull and transducer were fixed, and a 0.2-

mm needle hydrophone was placed within the skull for the purpose of mapping the transmitted sound field. The hydrophone position was controlled with the positioning system and its signal was conditioned with the pulser-receiver, digitized by the oscilloscope, and saved to a computer. At each position the transducer was first oriented perpendicular to the skull surface to achieve longitudinal mode transmission and the hydrophone was scanned along the plane parallel to the transducer face. Next, the transducer was incrementally rotated 5° relative to the skull surface from ±15-20° along the sagittal and coronal planes and a hydrophone scan was repeated for each angle, for a total of 43 scans. The six positions of the transducer relative to the skull consisted of the frontal bone lateral to the midline, posterior region of the parietal bone, above the suture of the parietal bones, the ventral region of the frontal bone, and the ventral region of the parietal bone below the cap. The super-suture positions were chosen purposefully to take advantage of the suture for distorting and spreading out the signal to maximize the interrogation volume for a given transducer. An example of this effect is shown in Fig. 2,

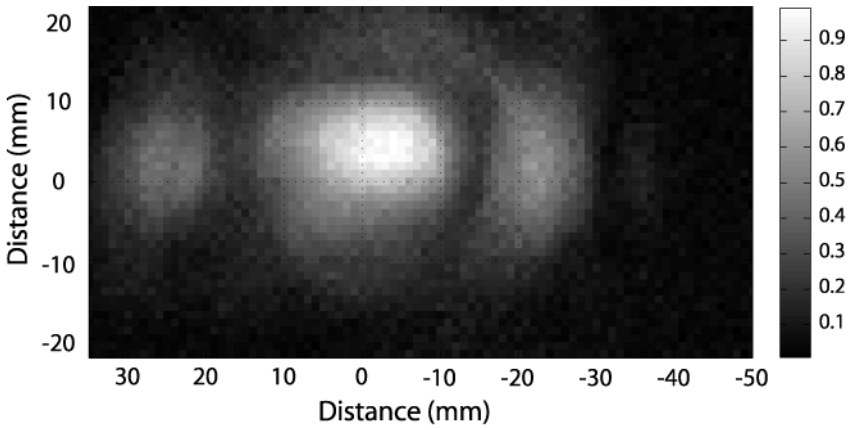

Figure 2: Normalized acoustic pressure inside the skull when transmission is primarily through the suture.

where a hydrophone scan was performed to measure the extent of the sound field when the transducer face was positioned parallel to the bone above the suture. The sound field is distinctly spread out with multiple lobes, illustrating the distortion effect caused by the suture. This effect is not desirable when a particular object needs to be localized in space, but is advantageous for identifying the presence regardless of its position.

Each individual scan was projected along its axis of propagation back to the skull surface using a numerical planar projection algorithm. This analysis provided a 3-D volumetric map containing the pressure amplitude at each position. The 43 amplitude maps were co-registered and combined into a single 3-D matrix based on the relative position of each measurement. From this dataset the volume inside the skull that contained signal within 20 dB of the peak pressure were compared to the total skull volume, shown in Fig. 3. This comparison provided a quantitative analysis of the

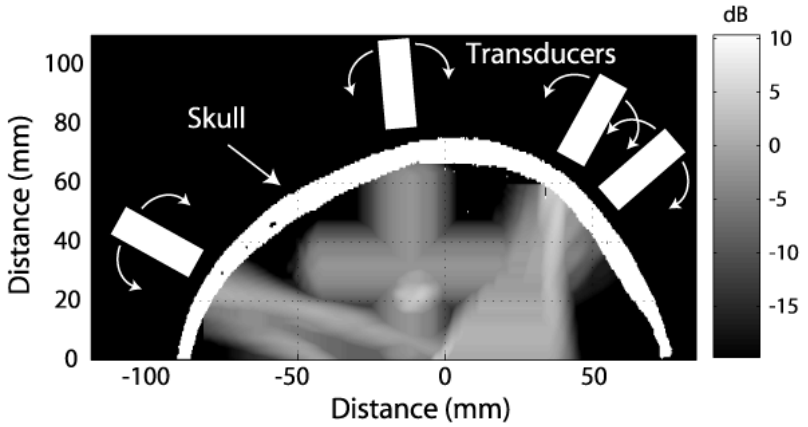

Figure 3: The projected interrogation area in the skull at the midline from the 6-transducer array, sagittal plane. The acoustic signals within 20 dB of the peak projected pressure are shown, with the skull and the transducers superimposed. The arrows denote

effective interrogation volume. Further insight into the interrogation region was obtained by examining the percent coverage along each coordinate axis, as shown in Fig. 4, providing a map of the regions that were not covered by the array. As can be seen in Figs. 3 and 4, the array interrogation volume is excellent near the center of the cranium cavity but decreases near the outer edges of the skull. Due primarily to the physical interference of the skull with the hydrophone, the measurements from which these projections are

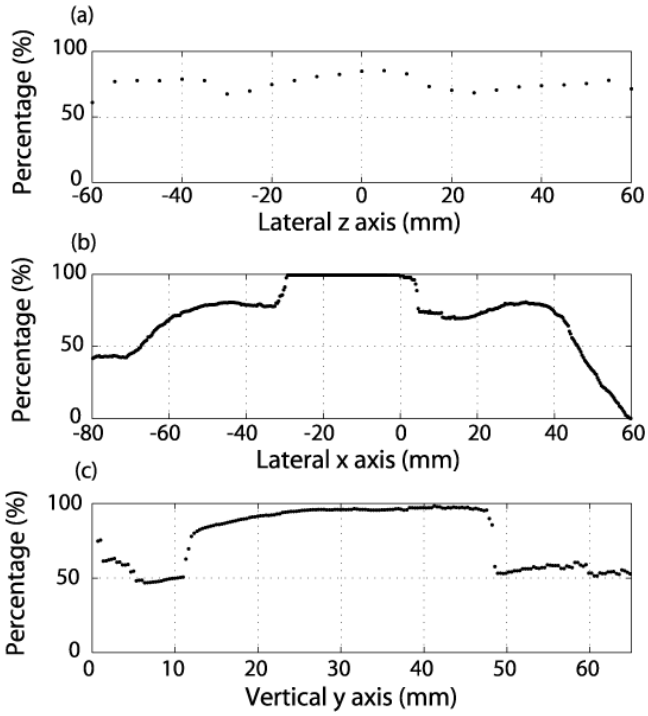

Figure 4: Percentage of ultrasound energy in the skull within 20 dB of the peak pressure

based include a relatively small angle variation. For this reason we expect that a larger

rotation angle will provide a significantly larger interrogation volume, particularly past the critical angle (~35°) when transmission through the skull will be primarily due to shear wave propagation. We will test this theory with the array and wider angles once the multi-channel pulser-receiver system is completed by scanning a spherical target inside the skull and examining the echoes received by the array. Additionally, we anticipate that the signal-to-noise ratio will substantially increase once the prototype pulser-receiver system is completed and implemented, increasing the interrogation volume.

Initative 4: System Electronics

Milestones 4, 7

In this period, the entire multi-channel pulser-receiver system was successfully constructed and tested. Figure 5 shows the overall block diagram for our system. As seen from Figure 6, three AA batteries will supply a 4.5V to the high voltage DC power supply, pulser and pulse generator. The pulser will provide the pulse generator two unipolar pulse train signals. The pulse generator converts the unipolar pulse trains into a bipolar pulse train signal that is then amplified using the variable high voltage (±60V to ±170V) provided by the high voltage DC power supply. The 1MHz bipolar pulse train signal created by the pulse generator is then delivered to the multiplexing system. The rotary dial connected to the multiplexing system allows for manual selection of the transducer that will transmit the signal. The transmit pulse from the multiplexing system is also connected to the sync input of the oscilloscope using a high impedance voltage probe. The pre-amplifier circuit is also connected to each transducer and conditions the signal received after. The conditioned signals from all transducers are then relayed to the oscilloscope. Finally, the oscilloscope will be connected to a computer through a GPIB cable that allows us to analyze the data using MATLAB.

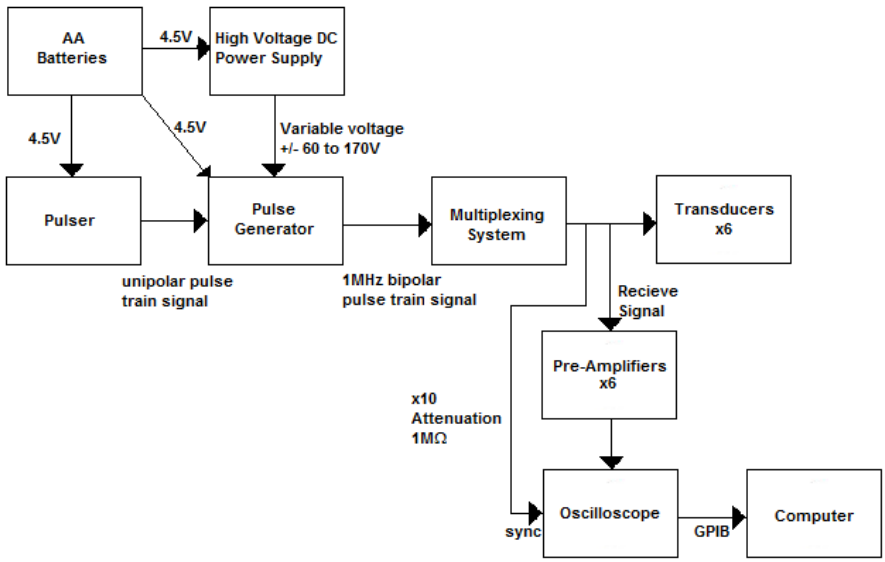

Figure 5. Block diagram of overall system.

High-Voltage DC Power Supply

The schematic for the High-Voltage DC Power Supply presented in Figure 6 was used to construct the power supply that provides power to the pulse generator through the outputs +HV and –HV. In order for the power supply to produce a stable output from the +HV and –HV outputs, it was necessary to reduce electrical noise that produced an unstable voltage at the outputs; an unstable high voltage can cause an uneven signal transmission from the pulse generator to the transducers. The electrical noise was being produced by two separate wires, one running from the DR pin of the LM3478 chip to the gate of the Q1 MOSFET and the other running from the FB pin of the LM3478 chip to the variable resistor VR1. In general, long wires can create unwanted impedances that can distort signals. The wire from the DR (drive) pin to the gate of the Q1 MOSFET was interrupting the signal from the pin and would cause the MOSFET to turn on and off when it was supposed to be kept on. We reduced the electrical noise by directly connecting the gate of the Q1 MOSFET to the DR pin and eliminating the use of a wire completely. The wire running from the FB (feedback) pin of the LM3478 chip to the variable resistor VR1 was also discarded and the resistor was directly connected to the FB pin. Connecting a variable resistor to the FB allows the output voltage to be read and controlled by an error amplifier and overvoltage comparator inside the LM3478 chip. The variable resistor, VR1, is also used to vary the output voltages, +HV and –HV, from ±60V to ±170V, where the positive voltages correspond to +HV and negative voltages correspond to -HV.

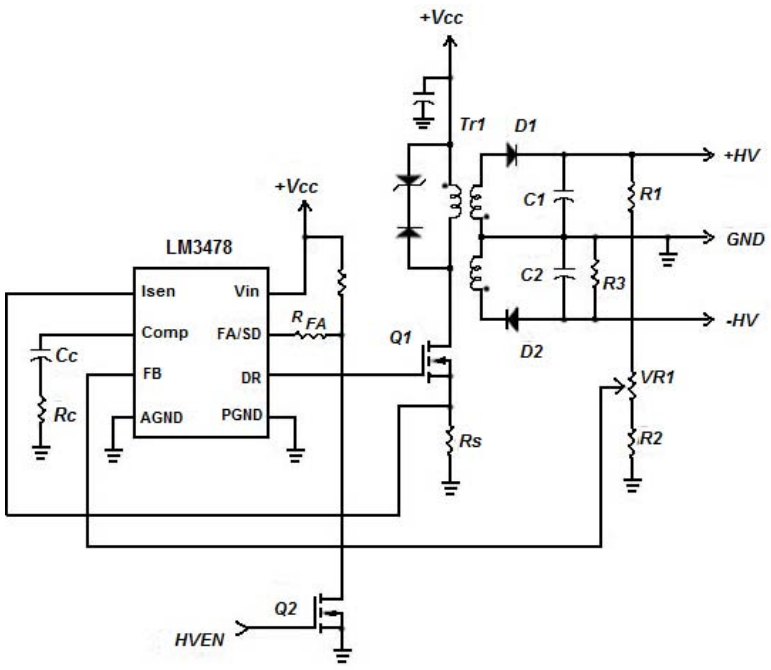

Figure 6. Circuit schematic of the high-voltage power supply.

The switching regulator controller chip (LM3478) requires a 12V +Vcc input; however, the voltage that is being supplied by the 3 AA batteries is 4.5V. In order to accommodate this, a miniature 1W, 3kV isolated unregulated DC/DC converter (DCH01) was used to step the voltage up from 4.5V to 12V. The LM3478 uses the 12V and steps it up to ±60V / ±170V made using the transformer Tr1.

The functionality of the high voltage DC power supply was tested by connecting 4.5V to the input of the DCH01 and observing the +HV and –HV outputs on the oscilloscope.

Bipolar Pulse Train Generator

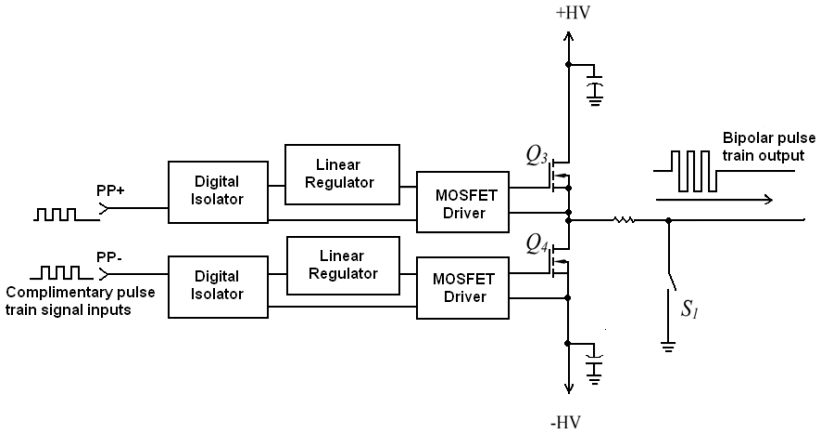

Figure 7. Schematic of the bipolar pulse train generator.

The bipolar pulse train generator was constructed using the schematic in Figure 7 to produce a 1MHz bipolar pulse train. To evaluate the functionality and detect fabrication errors, the pulse train was tested with an external function generator that supplied a 5V unipolar complimentary pulse train signal to the PP+ and PP- input terminals of the pulse generator. For testing purposes, an additional inverter was connected to the PP- input terminal to ensure that the pulse signals entering the input terminals were 180 degrees out-of-phase. An oscilloscope was used to visualize the signal produced by the pulse generator. The output signal was in the order of milliVolts, which was very small compared to our desired pulse train amplitude of ±170V; this amplitude was expected to be low since the pulse generator was not connected and powered by the high voltage power supply circuit. The high-voltage power supply is necessary to increase the amplitude of the pulse train.

The pulse generator needed to work properly before connecting it to the high-voltage power supply. If the pulse generator malfunctioned, it could cause a short circuit in the high-voltage power supply circuit and damage its Q1 MOSFET (Figure 5). Thus, an external voltage supply was first connected to the pulse generator in lieu of the high-voltage power supply to increase the amplitude of the pulse train. A 100Ω resistor was also connected in series with the output lead of the pulse generator in lieu of the transducers. During the initial test trials, as the external voltage supply increased its

voltage output to ±5V, the amplitude of the pulse train reached a limit of ±5V before signal distortion. Note that the amplitude of the external voltage supply output determines the amplitude to the bipolar pulse train. After the ±5V limit, the top MOSFET gate driver was damaged due to excess noise power entering the driver, which was caused by an inconsistent ground lead on the circuit board. More explicitly, the ground lead that spanned the circuit board was not entirely 0V: some areas were 0V, and areas further away from the ground source were above 0V. This "grounding" problem was due to the structure of the circuit board. To solve this problem, more areas of the ground lead were connected to one another using wires to ensure a constant 0V lead throughout the circuit board. After this adjustment, the external voltage supply was increased to its maximum output of ±31V without distortion of the bipolar pulse train signal. The pulse generator was then ready to be safely connected to the high-voltage power supply.

An additional part of the pulse generator was a switch circuit, denoted by S_1 in the pulse generator schematic of Figure 7. This switch circuit was provided by the lab and also successfully constructed in this period. The function of the switch circuit is to discharge the parasitic capacitors of MOSFETs Q_3 and Q_4 and the coaxial cable connecting to the transducers to zero potential. The discharge of these parasitic capacitors is important to prevent the pulse generator output from staying at high voltage for a long period of time when Q_3 and Q_4 are both turned off. Due to the design of the pulse generator, if these capacitors don't discharge, the high voltage can increase leakage current, which may be hazardous. Figure 4 shows the schematic of S_1. The parasitic capacitors are discharged via MOSFETs Q_5 and Q_6. The control input *IG* of this switch circuit is provided by an additional circuit, the pulser, which will be described in the next section. The switch circuit was tested by connecting to the output of pulse generator and successfully visualizing the desired three-cycle 1MHz bipolar pulse train output using an oscilloscope. The switch functioned as expected.

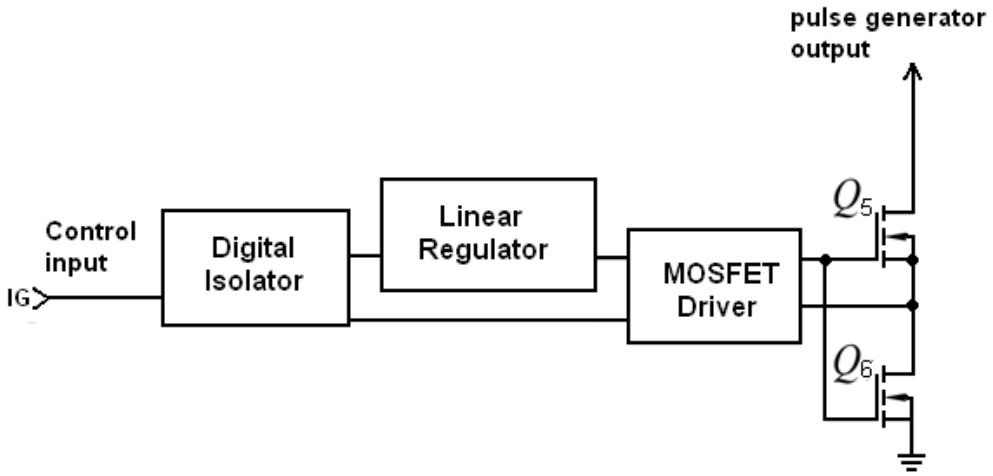

Figure 8. Schematic of the switch S_1

Pulser

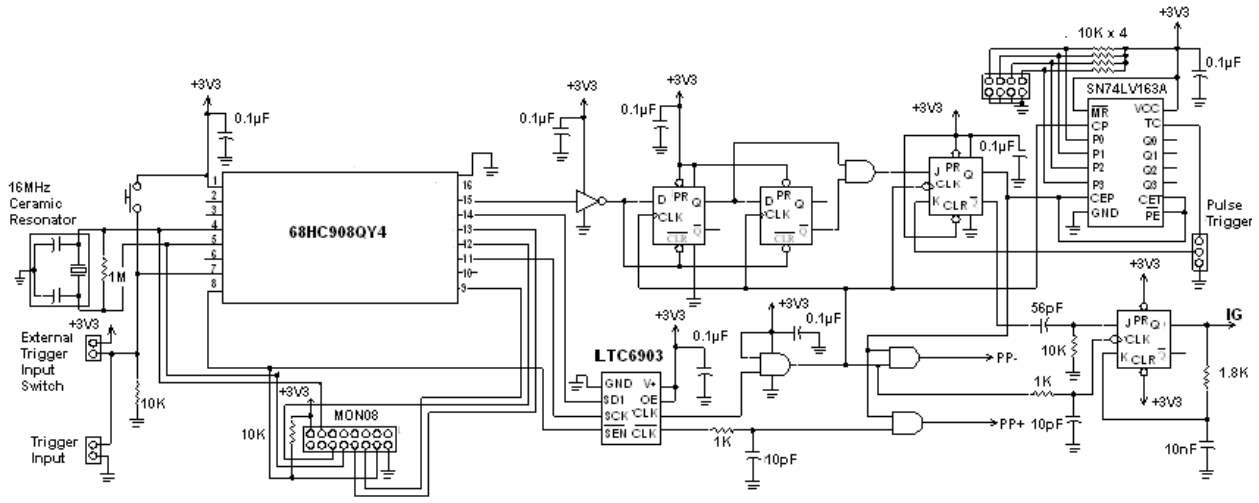

Figure 9. Schematic of the pulser.

Another recent addition to the project was the construction of the pulser, which produces the complimentary unipolar pulse train signals that will be supplied to the pulse train generator and provides the control input to switch S_1 shown in Figure 8. The schematic for the pulser shown in Figure 9 was pre-designed by the lab and provided for the project. The pulser includes a microcontroller (68HC908QY4) that was programmed via interface cable (MON08) to generate a pulse signal. The output of the microcontroller will then transmit to a programmable oscillator (LTC6903) that was programmed to modify the microcontroller pulse to multiple 1 MHz cycles. The microcontroller output also enters a series of logic gates (an inverter, four AND gates, two positive-edge triggered D-flip flops, and two negative-edge triggered JK-flip flops) and a binary counter (SN74LV163A) to limit the signal to three 1MHz cycles. Since three AA batteries supply 4.5V as the main voltage source to power the entire pulser-receiver system and the pulser circuit only needs to be powered by 3.3V, a voltage regulator (TPS71533DCKR) was added to step down the voltage supply from 4.5V to 3.3V.

The construction of the pulser was successfully completed in this period. Two 3.3V unipolar pulse train signals of three 1MHz cycles, which were 180 degrees out-of-phase and outputted at the PP+ and PP- terminals of the pulser, were verified using an oscilloscope. The external function generator and the additional inverter were disconnected from the PP+ and PP- input terminals of the pulse generator (Figure 7) and replaced by the pulser. From then on, the pulser supplies the complimentary unipolar pulse signals to the pulse generator. Moreover, a control signal to switch S_1 was outputted at terminal *IG*. After testing for the control signal using a multimeter, the pulser successfully provided the expected control signal to the switch. Overall, the pulser functioned as expected.

Switching System for Transducer Connection

The switching system was designed to include six channels that correspond to the six transducers that will be placed on different regions of the skull. Four designs were considered until one was found to be theoretically capable of transmitting a 1-MHz bipolar pulse train signal of amplitude ±170V to multiple transducers (Figure 10). The switching system was constructed with PCB relays (G6S-2G) and tested for switching capabilities by activating each PCB relay individually using an external voltage supply with a 12V DC output. To test the functionality of the PCB relays, an oscilloscope was used to ensure the transmission of a random ±5V square wave signal of 1MHz, which was supplied by an external function generator, through an activated PCB relay. Each PCB relay functioned as expected, transmitting the signal when activated.

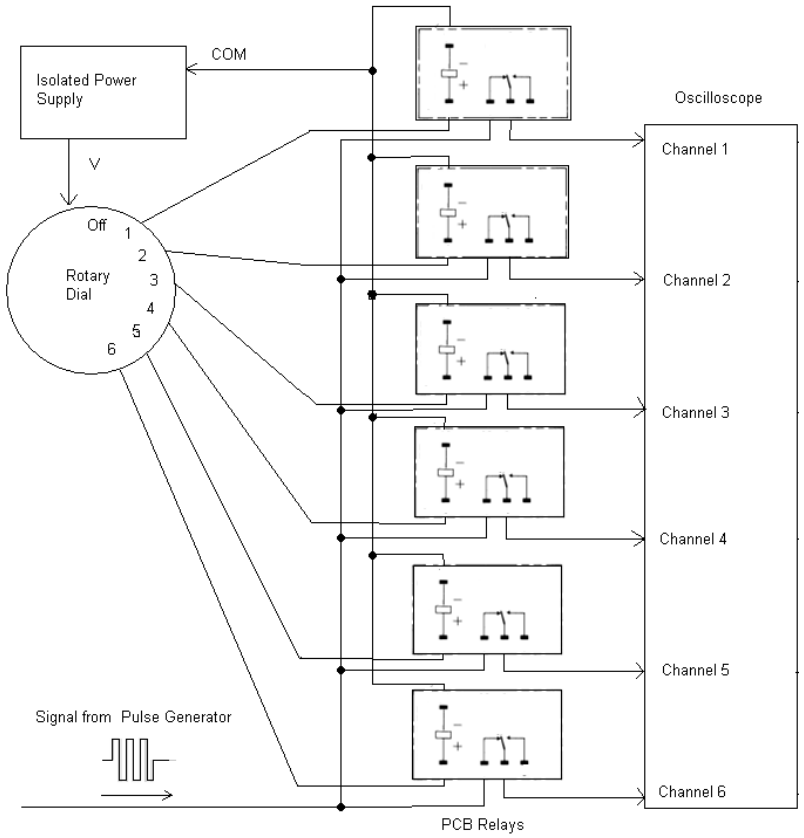

Figure 10. Final Design of the Multiplexing system employing 6 PCB relays.

Powering the Multiplexing System

The multiplexing system was ultimately devised as a 6 PCB relay array as shown in Figure 6. An isolated unregulated DC/DC converter was installed and connected to the

rotary dial. This DC/DC converter steps up the input voltage of 4.5V to 12V, the voltage required to turn on the PCB relays and provides a COM port for the PCB relays. The rotary dial is connected to the positive input ports of the 6 PCB relays allowing one PCB relay to turn on at a time. This component is functioning properly.

Figure 11. Pre-amplifier schematic.

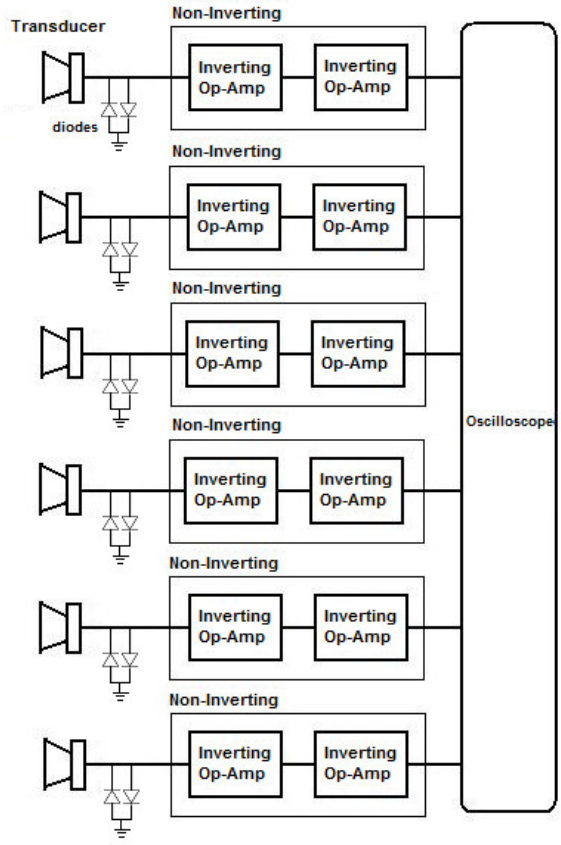

Pre-Amplifier

The return signals will be observed on an oscilloscope with 8-bit display resolution. The echo signals returned through the skull are expected to have low amplitudes, and observing a signal that does not fit the whole window can lead to digitization error. To avoid digitization error the return signal must be amplified to fit the whole window. A pre-amplifier, although not part of our original plan, was constructed to condition the received scattered wave signals. The amplifier was constructed using three quad operational amplifiers (LME49740). This chip was chosen because of its broadband response and the fact that each chip contains four operational amplifiers ideal to optimize space on the board. Twelve operational amplifiers were designed and constructed as inverting amplifiers to produce a gain of ten (20dB). For each channel, two amplifiers were then cascaded creating six non-inverting amplifiers that can produce a gain of 100 (40dB). The input of the six non-inverting amplifiers will be connected to the transducers and the output will be connected to the oscilloscope. Since the amplifiers will be connected to transducers that are emitting a high-frequency signal, two diodes (one in

reverse biased and one in forward biased) were placed between the transducers and the amplifier to protect the amplifier from getting saturated. The schematic for the pre-amplifiers is provided in Figure 11.

Evaluation of Range of Scattering Sizes

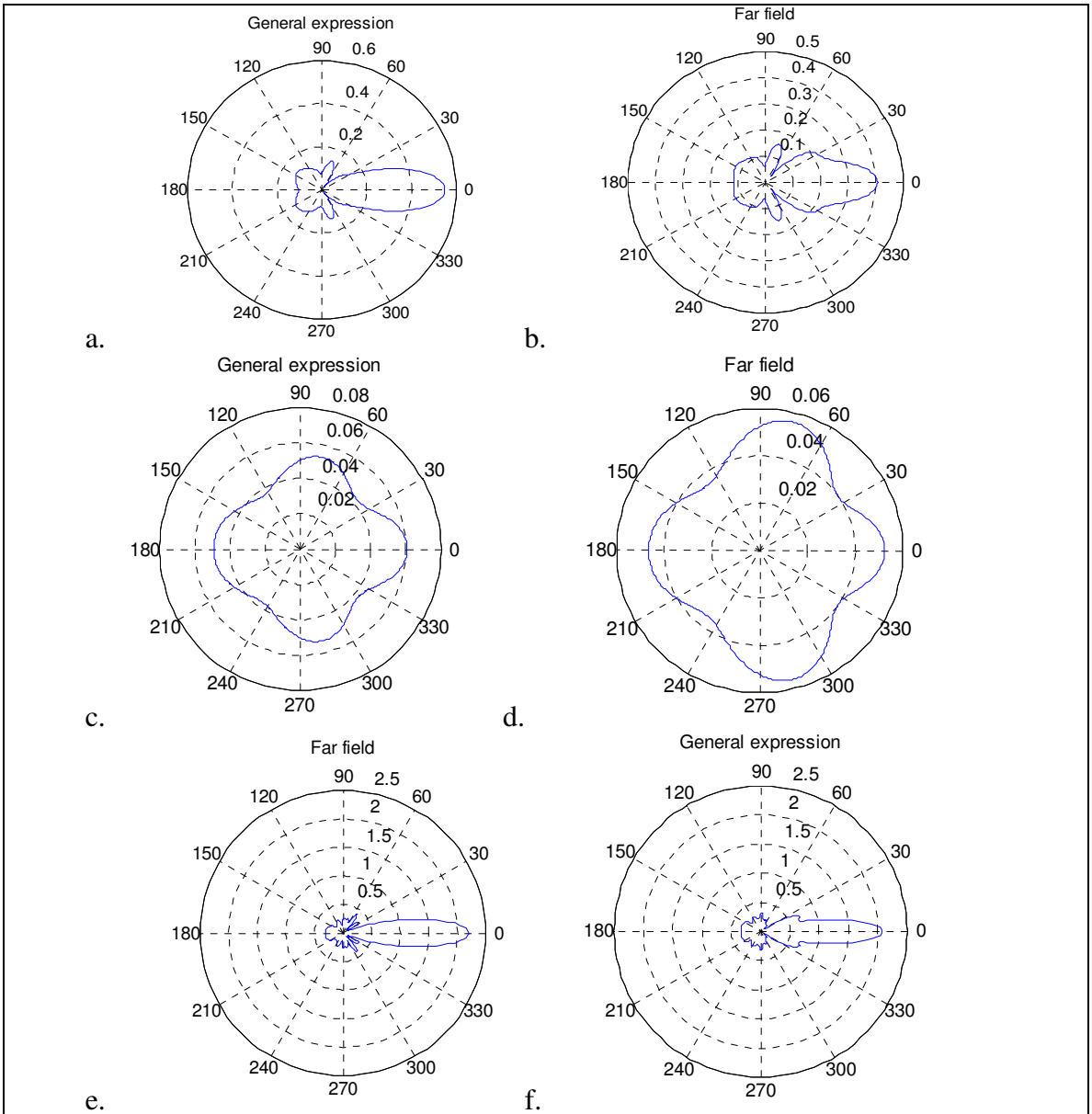

Figure 12. Computed amplitude of a pressure wave scattered by stainless steel sphere radii of (a) 0.5, (b) 1.25, and (c) 2.5 mm.

A MATLAB code was developed to simulate the pressure patterns of a range of sizes of stainless steel spheres from 1 to 5 mm in diameter using the scattering model for solid spheres described in Faran [*J. Acous. Soc. Am.* 23, 405-418 (1951)]. The computed scattering model simulates the relationship of the angular response and amplitude of the ultrasound echoes (due to the scatterers of various sizes) to the interrogation frequency of

1MHz. These MATLAB simulations will be used to extrapolate the pressure patterns that will be obtained from the actual experiments. The pressure patterns for solid spheres described in Faran were used to determine the accuracy of the code. Figure 6 shows the computed pressure patterns for scatterer radii of 0.5, 1.25, and 2.5 mm for the general expression for the outgoing scattered wave, $p_s = \sum_{n=0}^{\infty} c_n [j_n(k_s r) - jn_n(k_s r)] P_n(\cos\theta)$, and the far field expression for large distances from the sphere, $|p_s| \xrightarrow[r \to \infty]{} \frac{P_0}{k_s r} \left| \sum_{n=0}^{\infty} (2n+1) \sin\eta_n \exp(j\eta_n) P_n(\cos\theta) \right|$, described in Faran. The pressure in the scattered wave is plotted against the scattering angle θ. The incident sound is in the direction of angle θ=180°.

Figure 12 shows that the pressure patterns for the general expression and the far field expression for each scatterer size were fairly similar. Moreover, as the scatterer size increases the pressure of the scattered wave increases significantly more in the opposite direction of the incident wave (θ=0°) than in any other direction. For the pressure pattern of Figure 12(a) corresponding to the scatterer size of radius 0.5mm, it is viable to place transducers in every direction because the scattered pressure is almost omnidirectional. However, for the pressure pattern of Figure 12(c) corresponding to the scatterer size of radius 2.5mm, it is best to place a transducer at θ=0° because most of the scattered pressure is in that direction. Placing transducers in other directions will not provide significant results for determining the correct scatterer size. These computed pressure patterns provide benchmarks for determining the direction receiving transducers should be placed to obtain optimum results for the determination of scatterer size.

KEY RESEARCH ACCOMPLISHMENTS

Detailed accomplishments are provided throughout the body of the report. A summary of the key accomplishments are as follows:

- A transducer configuration has been developed that would allow approximately 80% of the brain to be measured in a single acquisition.
- Particles of <0.5 mm can be detected through the skull with the planned design and operational frequency
- A laboratory version of the computer interface has been written and implemented, including a user interface, and an analysis program
- The send-receive electronics have been completed and are currently being tested (approximately 3 months ahead of schedule)
- The transducer head is currently being constructed and matched.

REPORTABLE OUTCOMES

Year 1 of the project has been concerned with design, construction and optimization of a device and measurement method. Starting in the mid part of Year 2 work will turn more heavily to pre-clinical testing which is expected to provide data for publication.

CONCLUSION

Year one has progressed at, or slightly ahead of schedule, with major milestones during this period being met, while keeping in mind the overall goals of a device that is lightweight, portable, durable, battery-operated, easy to use and appropriate. The device builds upon a previously-built non-portable apparatus, which was clinically tested through the skull and verified against MRI measurements [6] and to detect fluid in the Maxillary sinus [7] and. Previously, we developed a computer-based ultrasonic pulser-receiver system that enables us to control the pulse train waveform and receive the echo signal through a software interface with the use of a personal computer. The next phase of the work will begin calibrating the device for a single function (foreign body detection), that will be begin clinical mockup testing this year.

REFERENCES

[1] G.T. Clement and K. Hynynen, "A non-invasive method for focusing ultrasound through the human skull," *Physics in Medicine and Biology*, vol. 47, Apr. 2002, pp. 1219-36.

[2] G.T. Clement, J. Sun, and K. Hynynen, "The role of internal reflection in transskull phase distortion," *Ultrasonics*, vol. 39, Mar. 2001, pp. 109-13.

[3] G.T. Clement, P.J. White, and K. Hynynen, "Enhanced ultrasound transmission through the human skull using shear mode conversion," *The Journal of the Acoustical Society of America*, vol. 115, Mar. 2004, pp. 1356-64.

[4] P.J. White, G.T. Clement, and K. Hynynen, "Longitudinal and shear mode ultrasound propagation in human skull bone," *Ultrasound in Medicine & Biology*, vol. 32, Jul. 2006, pp. 1085-96.

[5] P.J. White, S. Palchaudhuri, K. Hynynen, and G.T. Clement, "The effects of desiccation on skull bone sound speed in porcine models," *IEEE Transactions on Ultrasonics, Ferroelectrics, and Frequency Control*, vol. 54, Aug. 2007, pp. 1708-10.

[6] P.J. White, S. Whalen, S.C. Tang, G.T. Clement, F. Jolesz, and A.J. Golby, "An intraoperative brain shift monitor using shear mode transcranial ultrasound: preliminary results," *Journal of Ultrasound in Medicine: Official Journal of the American Institute of Ultrasound in Medicine*, vol. 28, Feb. 2009, pp. 191-203.

[7] S.C. Tang, G.T. Clement, and K. Hynynen, "A computer-controlled ultrasound pulser-receiver system for transskull fluid detection using a shear wave transmission technique," *IEEE Transactions on Ultrasonics, Ferroelectrics, and Frequency Control*, vol. 54, Sep. 2007, pp. 1772-83.

APPENDIX

Milestone	Time Period	Metric
M1. Transducer Design	Month 4	Coverage across skull
M2. Simulation of Echoes	Month 9	Sensing of 1 mm particles
M3. USB Interface	Month 12	Working device
M4. GUI	Month 12	Completed Software
M5. Analysis Algorithm	Month 18	Alpha version, ready for lab use
M6. Transducer Head	Month 15	Completed, ready for lab use
M7. Transducer Matching	Month 18	Complete and tested circuit
M8. Transskull Field Maps	Month 21	Measurement, 3 *ex vivo* skulls
M9. Phantom Construction	Month 21	3 phantoms built/characterized
M10. Lab Study	Month 24	Measurement 10 ex vivo skulls
M11. Skull variation study	Month 28	10 skulls, with 1 brain phantom
M12. Foreign body local. study	Month 36	2 Skulls, with 10 separate brain phantoms